THE JOURNAL OF COMPARATIVE NEUROLOGY 422:415–428 (2000)

Comparative Analysis of Dendritic Architecture of Identified Neurons Using the Hausdorff Distance Metric

ADI MIZRAHI,[1] EYAL BEN-NER,[2] MATTHEW J. KATZ,[2] KLARA KEDEM,[2]
J. GUSTAVO GLUSMAN,[1] AND FREDERIC LIBERSAT[1]*
[1]Zlotowski Center for Neuroscience and Department of Life Sciences, Ben-Gurion University of the Negev, Beer-Sheva, 84105 Israel
[2]Department of Mathematics and Computer Science, Ben-Gurion University of the Negev, Beer-Sheva, 84105 Israel

ABSTRACT

Dendritic trees often are complex, three-dimensional structures. Comparative morphologic studies have not yet provided a reliable measure to analyze and compare the geometry of different dendritic trees. Therefore, it is important to develop quantitative methods for analyzing the three-dimensional geometry of these complex trees. The authors developed a comparison measure based on the Hausdorff distance for comparing quantitatively the three-dimensional structure of different neurons. This algorithm was implemented and incorporated into a new software package that the authors developed called *NeuroComp*. The authors tested this algorithm to study the variability in the three-dimensional structure of identified central neurons as well as measuring the structural differences between homologue neurons. They took advantage of the uniform dendritic morphology of identified interneurons of an insect, the giant interneurons of the cockroach. More specifically, after establishing a morphometric data base of these neurons, the authors found that the algorithm is a reliable tool for distinguishing between dendritic trees of different neurons, whereas conventional metric analysis often is inadequate. The authors propose to use this method as a quantitative tool for the investigation of the effects of various experimental paradigms on three-dimensional dendritic architecture. J. Comp. Neurol. 422:415–428, 2000.

Indexing terms: three-dimensional reconstruction; dendritic trees; geometry; morphometry

The three-dimensional (3D) structure of a neuron is critical in determining how synaptic inputs are integrated to produce a coded output (Segev, 1992; Yuste and Tank, 1996; Segev and Rall, 1998). It is therefore essential to develop the methodology and tools to quantitatively analyze the 3D geometry of dendritic arborizations of neurons. Such tools would be extremely useful to identify and quantify the changes in dendritic architecture during development and aging or as result of experimental treatment.

Metric analysis of dendritic tree structures is used as a tool for determining the structural changes in dendritic arborizations (Uylings et al., 1986). However, because a single parameter cannot describe all geometric properties of a dendritic tree, it is necessary to use several parameters to describe neuronal architecture (Uylings et al., 1986; Verwer and van Pelt, 1986). A common quantitative method that is used to analyze the spatial geometry of neurons is the Sholl analysis (Sholl, 1953). The Sholl analysis provides information about the spatial distribution of the dendritic arborizations of a neuron. Briefly, it consists of counting the number of occurrences of a given morphometric parameter of the dendritic tree (i.e., branch points, segment length, etc.) along concentric spheres separated by a fixed number of microns. However, one can imagine two neurons with similar morphometric parameters but with different architecture (Fig. 1A). Thus, Sholl analysis and standard metric parameters are not sufficient tools for measuring resemblance in neuronal architecture. More recently, fractal analysis has been used to

Grant sponsor: Israel Science Foundation; Grant number; 9001/95; Grant sponsor: Israel Science Foundation.

*Correspondence to: Frederic Libersat, Department of Life Sciences, Ben-Gurion University of the Negev, P.O. Box 653, Beer Sheva, 84105 Israel. E-mail: libersat@bgumail.bgu.ac.il

Received 30 November 1999; Revised 29 February 2000; Accepted 1 March 2000

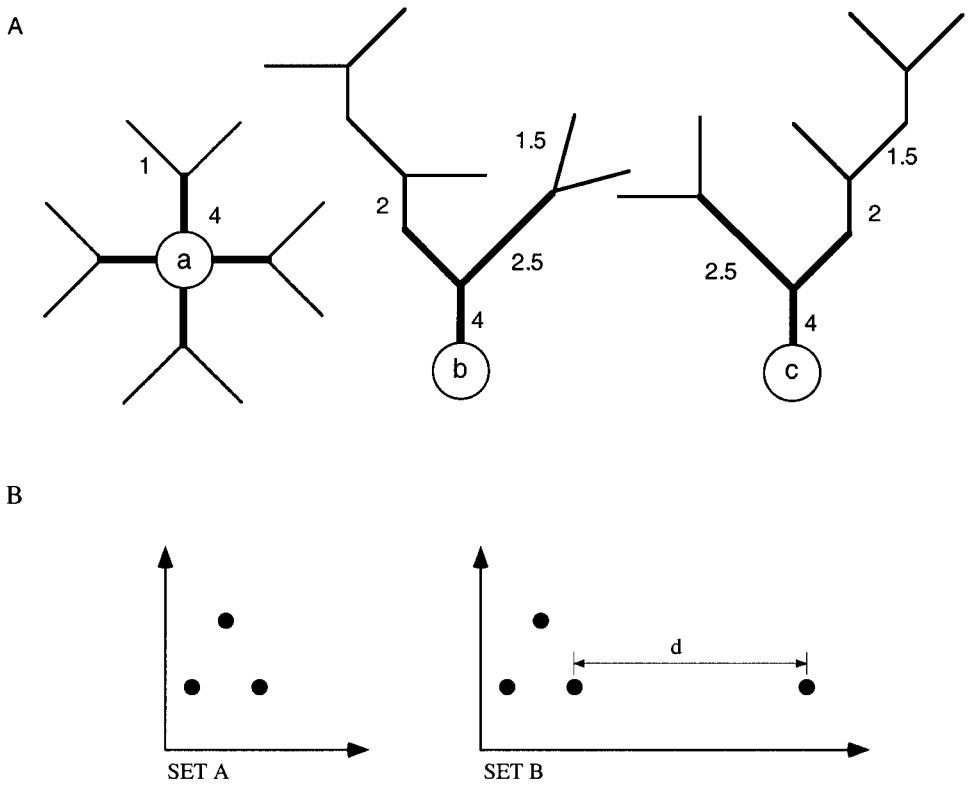

Fig. 1. **A:** Schematic example of three dendritic trees with similar standard morphometric parameters. Cell a and cell b share the same number of branch points, total length, and surface area (denoted by numbers, which represent thickness). The cells differ in the number of end points, "path distance," "parent-daughter ratio," and "number of dendrites." Cell b and cell c share all standard measurements mentioned above. **B:** The principle of the Hausdorff distance (HD). The set shown on the left (SET A) consists of 3 points that match exactly the group of 3 points in the set on the right (SET B). Therefore, the HD between SET A and SET B is 0 (or SET A = SET B). By contrast, SET B is a set of 4 points, one of which is at a distance (d) away from the closest point in SET A. Therefore, the HD between SET B and SET A is "d".

evaluate the complexity of neuronal dendritic arborization (Smith et al., 1989, 1996). Fractal dimension is a measurement of complexity that is useful for describing the shapes of objects quantitatively, because one can associate fractal dimension values with complexity of form. Although the fractal dimension can be useful to evaluate the complexity of a 2D or 3D object, it cannot be used for determining the degree of resemblance between two dendritic trees. The purpose of the current study was to rectify this deficiency by developing an efficient tool with which to analyze the degree of resemblance between neuronal arborizations.

One area of research in computational geometry is to devise metrics for determining the degree of similarity between two images. Determining the degree of resemblance between two shapes can be approached by using a distance measure, which is based on the Hausdorff distance (HD; Huttenlocher and Kedem, 1990; Huttenlocher et al., 1991; Chew et al., 1997; Chew and Kedem, 1998). It has been demonstrated that the HD is a suitable measure for image comparison (Huttenlocher et al., 1993).

To evaluate the effects of specific factors on the 3D geometry of neurons, it would be of great advantage to use neurons with a uniform, 3D architecture. These could be used as templates for examining the effect of various experimental manipulations on their geometry. Identified neurons are a prevalent feature of the invertebrate nervous system: These neurons show a characteristic morphology and physiology. A very well-studied example of such neurons is the abdominal giant interneurons (GIs) of crickets and cockroaches (Mendenhall and Murphey, 1974; Daley et al., 1981). The GIs are a small group of individually identified neurons, and considerable information is available on their sensory input, motor output, and cellular properties (Daley et al., 1981; Blagburn and Beadle, 1982; Ritzmann, 1984; Bacon and Blagburn, 1992; Blagburn et al., 1996; Hill and Blagburn, 1998).

In this study, we present a new method for the quantitative comparison of 3D dendritic structures based on the HD. We tested the practicality of this method by computing the variability in the 3D structure of dendritic trees of consistently identifiable central neurons. A preliminary report of this data was presented previously in abstract form (Mizrahi et al., 1999).

MATERIALS AND METHODS

Animals

Freshly moulted adult cockroaches (*Periplaneta americana*) from the laboratory colony were used in all experiments. Cockroaches were raised in plastic barrels, kept at 27–32°C, and provided with water and cat chow as needed.

Staining and histology

Cockroaches were pinned dorsal side up on a recording platform after cutting the legs and wings. Then, the ventral nerve cord was exposed from the second abdominal ganglion (A2) to A6, as described previously (Libersat, 1992). GIs were impaled in the axon between the A5–A6 connectives with a glass microelectrode (resistance, 20–40 MΩ) filled with 2% neurobiotin in 1 M KCl. Neurobiotin was ionophoresed (20 nA depolarizing pulses; duration, 200 msec; frequency, 4 Hz) into the axon for 30–60 minutes followed by a diffusion period of 1 hour. The abdominal nerve cord was dissected out into a Sylgard dish and fixed in 2.5% glutaraldehyde in Millonig's buffer (MB), pH 7.4. The nerve cord was then dehydrated in 30%, 50%, 70%, 90%, and 100% ethanol for 10 minutes each; transferred to propylenoxide; and then rehydrated into MB. To facilitate the penetration of molecules into the tissue, the nerve cord was incubated in collagenase/dispase (1mg/ml) in MB at 37°C for 1 hour. The tissue was then reacted with avidin-conjugated horseradish peroxidase (Vectastatin ABC kit; Vector Laboratories, Burlingame, CA) diluted in MB with 1% Triton-X overnight. Subsequently, the tissue was presoaked with 3,3′-diaminobenzidine tetrahydrochloride (DAB; Isopac; Sigma, St. Louis, MO) diluted in a solution of MB containing 0.25% $NiCl_2$, 0.25%$CoCl_2$, and 1% Triton-X at 4°C in the dark and then oxidized with 0.015% hydrogen peroxide. After the DAB procedure, the tissue was mounted with Permount (Fischer Scientific, Fair Lawn, NJ) onto custom-made, 0.5-mm-thick slides.

3D reconstruction

Each neuron was visualized through a BH-2 Olympus microscope (Olympus, Tokyo, Japan) with an oil-immersion lens (×100; NA, 0.8; working distance, 0.66 mm). The neurons were reconstructed with a commercial, 3D reconstruction system (Neurolucida; Microbrightfield Ltd., Brattleboro, VT). Only neurons that were filled to the tip of the finest distal dendrites were reconstructed. Each reconstructed neuron consisted of ≈ 4,000–6,000 digitized points, each represented by X, Y, and Z coordinates and the diameter of the tapered branch. Basic morphometric parameters were computed with the Neurolucida Explorer software (version 3; Microbrightfield Ltd.). Comparative measurements were computed with the NeuroComp software developed in our laboratory.

The photomicrograph shown in Figure 2A was taken through a compound light microscope (BH2; Olympus) equipped with integrated control of digital camera and microscope focal-positioning equipment using a ×10 objective. Optical sections were acquired at 5-μm steps (in the Z axis) and were collapsed as a projection image by using the average command of the imaging software (IPLab Spectrum). The photomicrograph shown in Figure 2A is a scanned image of a photomicrograph that was taken through the compound light microscope (BH2; Olympus) with an Olympus SC35 camera.

Alignment and scaling

The alignment of the GIs is a two-step procedure. First, the GIs were aligned by a rotation parallel to the posterior-anterior axis according to measures of the three radii of the ganglion, as described by Jacobs and Nevin (1991). Then, for cell-cell comparison with the Hausdorff method, two GIs were aligned at their respective junctions between the link segment, the dendritic tree, and the axon (Fig. 6). Because we could not find any correlation between any given morphometric parameter and ganglion size, we did not rescale the neurons. The histologic procedure caused a uniform shrinkage of roughly 30%, which was not corrected.

Morphometric analysis

GIs were examined quantitatively in several ways: first, by the metric parameters number of branches, total dendritic length, and total dendritic surface area and fractal dimension. The general distribution of dendritic trees was analyzed by using the Sholl concentric-spheres method (Sholl, 1953). The spheres were centered at the alignment node, spaced apart by 20 μm (Fig. 5A) throughout the dendritic tree, and the number of branching points within each sphere was counted. The spatial distribution of the GIs was analyzed by using the HD for comparing pairs of dendritic trees. A software package, NeuroComp, was developed based on this method [more details concerning this software package can be found at http://www.cs.bgu.ac.il/≈benner/project/ (Unix)]. The main features of the package are the comparison between pairs of dendritic trees and the visualization of the compared neurons in various ways: 3D appearance, space occupancy by the two neurons (logic OR), space occupancy by both neurons (logic AND), and space occupancy by only one neuron (logic XOR). The software also enables the user to manipulate and view the neuron's position in space. The software was developed in C++ on Unix and on WinNT. Below, we describe the HD for measuring resemblance between dendritic trees.

HD and its variations

Definition: The symmetric HD [H(A,B)] between two point sets, $A = (a_1,\ldots,a_n)$ and $B = (b_1,\ldots,b_m)$, is computed by taking the maximum of what is called the two "one-way" HDs,

$$H(A,B) = \max(h(A,B),h(B,A)), \quad (1)$$

in which the one-way HD from A to B is defined as

$$h(A,B) = \max_{a_i \in A} dist(a_i,B), \quad (2)$$

where the distance between a point a_i and the set B is defined as

$$dist\ (a_i,B) = \min_{b_j \in B} \rho(a_i,b_j), \quad (3)$$

and $\rho\ (a_i,b_j)$ is the distance between points a_i and b_j.

The function h(A,B) is the *one-way* HD from A to B. It is the distance of the farthest point of A from any point in B. The one-way HD is not symmetric, whereas H(A,B) is symmetric. However, knowing the values of h(A,B) and h(B,A) gives more insight into the amount of inclusion of A in B, and vice versa. The HD principle is illustrated in Figure 1B, in which two sets of points in the plane, A and B, are shown. A consists of three points, and B consists of four points. The three points on the left side of B match A exactly, but B has an outlying point at a distance d from

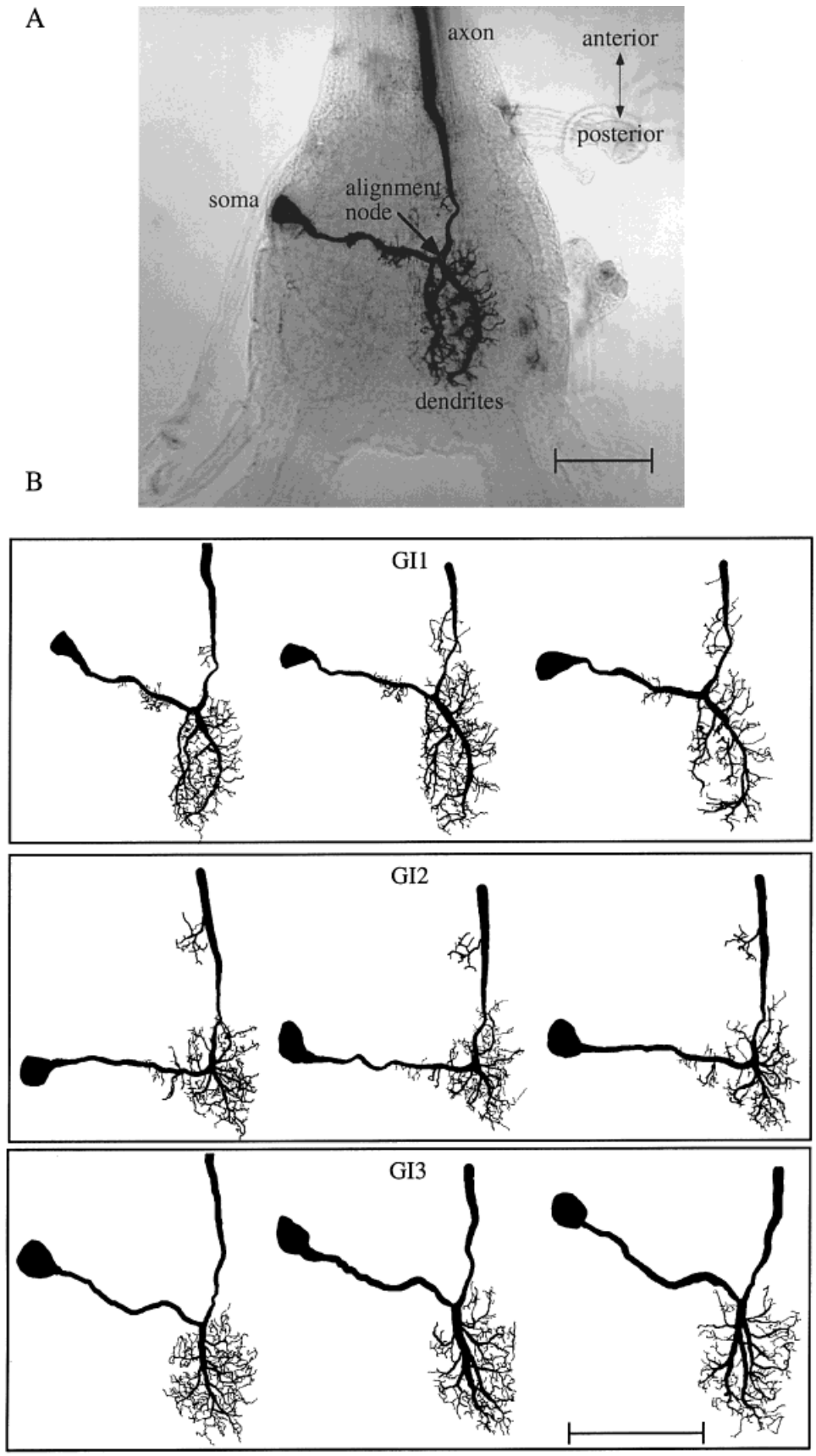

Fig. 2. Identified giant interneurons (GIs). **A:** Photomicrograph of a neurobiotin-labeled right GI_1 in a wholemount of the last abdominal ganglion shown in the dorsal view. **B:** Three examples of each reconstructed GI (GI_1, top; GI_2, middle; GI_3, bottom) shown in the dorsal view. The left GI_1 is the same neuron shown in A. Scale bars = 150 μm in A; 250 μm in B.

the closest point in A. According to Equation 2, h(A,B) = 0, whereas h(B,A) = d: Thus, H(A,B) = d.

A variation of this method takes into account that the measured coordinates of the points are imprecise within a certain tolerance, ε. A point a_i is considered identical to a point b_j if the distance $\rho(a_i,b_j)$ is $< \varepsilon$ (we say in this case that a_i and b_j are "ε-close"). We define p(A,B) as the percent of points of A that are ε-close to B and p(B,A) as the percent of points of B that are ε-close to A. Compatible with Equation 1, the symmetric measure P(A,B) is

$$P(A,B) = \min(p(A,B),p(B,A)). \quad (4)$$

In the example shown in Figure 1B, if ε is set to a value $<$ d, then p(A,B) is 100%, and p(B,A) is 75%. If ε is set to a value $>$ d, then p(A,B) and p(B,A) are 100%. We define this variation of the HD distance as the Hausdorff match (HM).

Implementing the HM between dendrites

After aligning two dendritic trees, we take the 3D bounding box, which includes the dendritic trees, and divide it into "voxels" of 2 μm^3 to create a 3D grid within the bounding box. Then, each dendritic branch of each tree is converted into a set of points that fills the branch volume, as shown in Figure 6. All points that fall in the same voxel are reduced to a single point. Such sets of points are referred to as "dendritic clouds." All HM comparisons discussed below use dendritic clouds as their input files.

Given two dendritic clouds, A and B, we compute for each point $a_i \in A$ the distance da_i to its closest point in B. Similarly, for each point $b_i \in B$, we compute db_i, the distance to its closest point in A. The largest number in the set $\{da_i\}$ is the one-way HD from A to B. We calculate $\{da_i\}$, in percent values, for different ε and construct a graph for different ε. Interpreting this in terms of ε-closeness, for any given distance ε, the graph gives us the percentage of points of A that are within distance ε of B. In the same, way we build the graph for the set B (Fig. 7).

Given the limited ability to fine tune our rotational alignment, we compute p(A,B) and p(B,A) for a small number of spatial rotations of the cell. Our computation looks for the best result in ±7° in all axes.

RESULTS

Quantitative morphometric analysis of the GIs using standard methods

A qualitative description of the morphology of the GIs has been provided by Daley et al. (1981). The GIs are located in the last or most posterior ganglion of the nerve cord. This ganglion results from the fusion of the five most posterior segmental abdominal ganglia. The GIs are subdivided into two functional groups: the ventral GIs (vGIs) and the dorsal GIs (dGIs). Each group consists of three pairs of bilateral cells. Each neuron's morphology was described from 2D projections that were generated from camera-lucida drawings of cobalt-stained neurons. This work describes qualitatively and quantitatively the architecture of the three ventral GIs (GI_1, GI_2, and GI_3). We examined the morphology of these three identified GIs by sampling 26 neurons (n = 5 GI_1, n = 16 GI_2, and n = 5 GI_3).

A neurobiotin-stained GI_1 in wholemount is shown in Figure 2A. The GIs are monopolar neurons with a soma contralateral to the axon and dendritic tree. The soma is located outside the neuropil on the edge of the ganglion. It is connected to the axon and the dendritic tree by a neurite that we refer to as the *link segment*. The somata of GI_1 and GI_3 are located in the anterior part of the ganglion, whereas the soma of GI_2 is found in a more posterior location. The dendritic trees of the GIs are distributed mainly in the posteromedial part of the neuropil and do not cross to the opposite side of the ganglion. However, some short, individual dendrites arise from the link segment. In addition, a small neuronal tree branches out of the axon in the anterior part of the ganglion. These neuronal processes are not included in our quantitative analysis, because this study focused on the dense dendritic tree.

Three reconstructed examples of GI_1, GI_2, and GI_3 from different animals are presented in Figure 2B as projection images in the dorsal view (GI_1, top; GI_2, middle; GI_3, bottom). Based on these examples, it is apparent that the architecture of each GI is unique, thereby illustrating the concept of consistently identifiable neurons. Dendrograms of each GI provide a 2D schematic representation of the branching structure of the dendritic tree (Fig. 3). GI_1 shows two main primary dendrites. The largest dendritic tree projects posteriorly, and the smaller dendritic tree projects dorsally. The larger dendritic tree of GI_1 has a maximum branching order of 26 ± 7 (average ± S.D.; n = 5) and a maximum path distance from the dendritic root to the most distal dendrite reaching values of 350–400 μm (Fig. 3A). The dendritic tree of GI_2 is more compact, with four to five major primary dendrites (projecting radially from the main dendritic root). The larger dendritic tree of GI_2 exhibits a maximum branch order of 17 ± 1 (average ± S.D.; n = 10), where most dendrites reach approximately 200 μm in their maximum path distances (Fig. 3B). Finally, GI_3 exhibits only one large dendritic tree. The maximum branching order of the single dendritic tree is 18 ± 3 (average ± S.D.; n = 5). Path distances of the dendritic tree of GI_3 may reach over 400 μm (Fig. 3C).

A quantitative analysis comparing the number of branch points, total lengths, and total surface areas is presented in Figure 4. Despite the fact that these cells are different morphologically, we found no significant differences in these parameters among the three neurons [analysis of variance (ANOVA); $P > 0.05$]. Variability of the metric parameters ranged from a minimal coefficient of variance of 0.07 (surface area of GI_3) to a maximum of 0.35 (surface area of GI_2). Based on these metric parameters, we could not identify any morphometric parameter that was more variable or less variable than the others.

To compare the geometry of the GIs, we analyzed the gross spatial distribution of the dendritic trees of GI_1, GI_2, and GI_3 by using Sholl's concentric-spheres method (Fig. 5). The dendritic tree of GI_2 is the most compact of all three GIs, because it spreads over a radius of only 200 μm; the density of the number of branching points peaks at a radius of 80 μm from the center. The dendritic branching points of GI_1 and GI_3 are distributed more uniformly throughout the tree and spread over a maximum distance of 320 μm and 280 μm, respectively. Analysis of other metric parameters of the dendritic trees (i.e., number of intersecting segments, length, and surface area) within the Sholl spheres showed a distribution comparable to

that of the number of branching points for these three neurons (data not shown). The results from the Sholl analysis indicated some differences in the general spatial distribution between GI_2 and the other two GIs (GI_1 and GI_3). In contrast, this analysis did not reveal any major difference between GI_1 and GI_3.

Finally, we also analyzed the fractal dimension (FD) of the GIs by using the box counting method (Neuroexplorer version 3.10) as an additional tool to compare the architecture of the dendritic trees of the GIs. We found no significant difference (t-test; $P > 0.7$) between the GI_1 group (FD = 1.22 ± 0.04), the GI_2 group (FD = 1.21 ± 0.04), and the GI_3 group (FD = 1.20 ± 0.03).

Quantitative morphometric analysis of the GIs using the HM method

First, we transform each reconstructed dendritic tree into a set of points that we refer to as a *dendritic cloud* (Fig. 6). Each cloud point is assigned an *address* (x, y, z coordinates) in the 3D grid. These dendritic clouds are the input files for the HM comparison. The need for an unbiased, quantitative tool to measure resemblance between dendritic trees is illustrated in Figure 7A for three dendritic trees of GI_2. How much do these cells resemble one another? It is difficult to establish the degree of resemblance among these cells. To overcome this difficulty, we analyzed the architecture of these neurons by using the HM method. In this version, we measured the percentage of points of one cell that lay within a given distance from the points of the other cell (ε-closeness): We call it the HM. If the HM is high for a relatively small distance ε, then the two dendritic trees are similar in shape. Because the test described above is not symmetric, each pair is compared twice, and the lower HM is then chosen as the symmetric HM for the given pair. For example, consider the two cells from Figure 7A (cells a and b). Comparing cell a with cell b is different than comparing cell b with cell a, as shown by the two curves of the "one-way" HM test in Figure 7B. In this case, at any checked distance ϵ, cell a has more overlapping points in cell b (Fig. 7B, "a in b") than b has in a (Fig. 7B, "b in a"). Thus, the symmetric HM test for these two cells will be the "lower" value, or the "b in a" curve. The resemblance between dendritic trees a and b at an ε-closeness of 2 voxels is 32% (Fig. 7B, solid circle), and the resemblance at an ε-closeness of 5 voxels is 62% (Fig. 7B, open circle). The HM curves for the three examples in Figure 7A are shown in Figure 7C. By using this test, cells b and c have higher resemblance than cells a and b or than cells a and c.

We tested the HM method on neurons that have visible morphologic differences, such as GI_1 and GI_3, to determine whether the HM measure discriminates between these neurons, in which morphometric comparison (Fig. 4) and Sholl analysis (Fig. 5B) did not. Figure 8 shows that the HM test detected the differences between these two neurons. Comparison of all possibilities between neurons from the same group, (i.e., GI_1 vs. GI_1 and GI_3 vs. GI_3; n = 5 for each) yielded high similarity values (Fig. 8, triangles; each curve represents the average data calculated from 20 comparison curves). In contrast, comparison between different groups (i.e., GI_1 vs. GI_3) yielded lower similarities (Fig. 8, circles; data calculated from 50 comparison curves). An analysis of covariance (ANCOVA) showed no significant difference ($P > 0.05$) between the two intragroup curves (GI_1 vs. GI_1 and GI_3 vs. GI_3). In contrast, there was a significant difference ($P < 0.01$) between each intragroup curve and the intergroup curve (GI_1 vs. GI_3). For example, at an ε-closeness of 5 voxels, the similarities of the intragroup are 63% and 76%, whereas the similarity

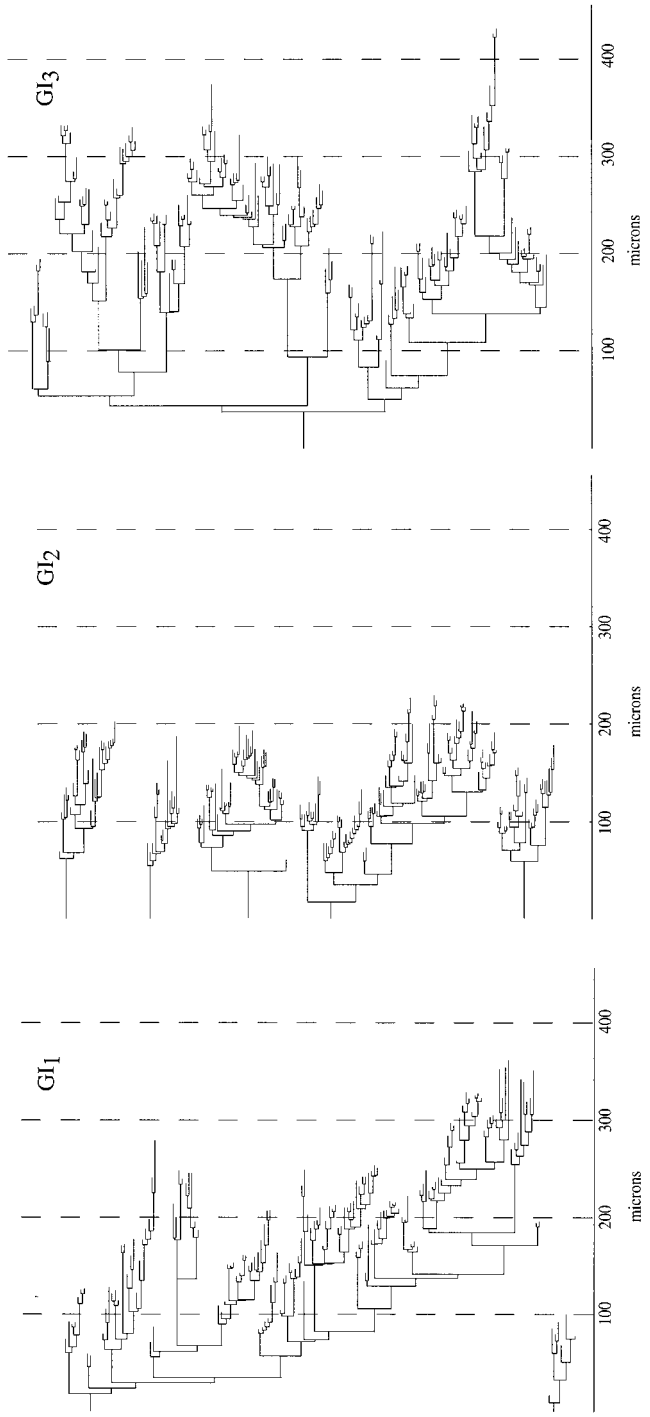

Fig. 3. Dendritic trees of the three GIs. Left: Dendograms showing schematic representations of the branching pattern of the GIs shown on the right. Right: Representations of the dendritic trees of the three GIs that were made with the NeuroComp software. **A:** GI_1. **B:** GI_2. **C:** GI_3. Scale bar = 100 μm.

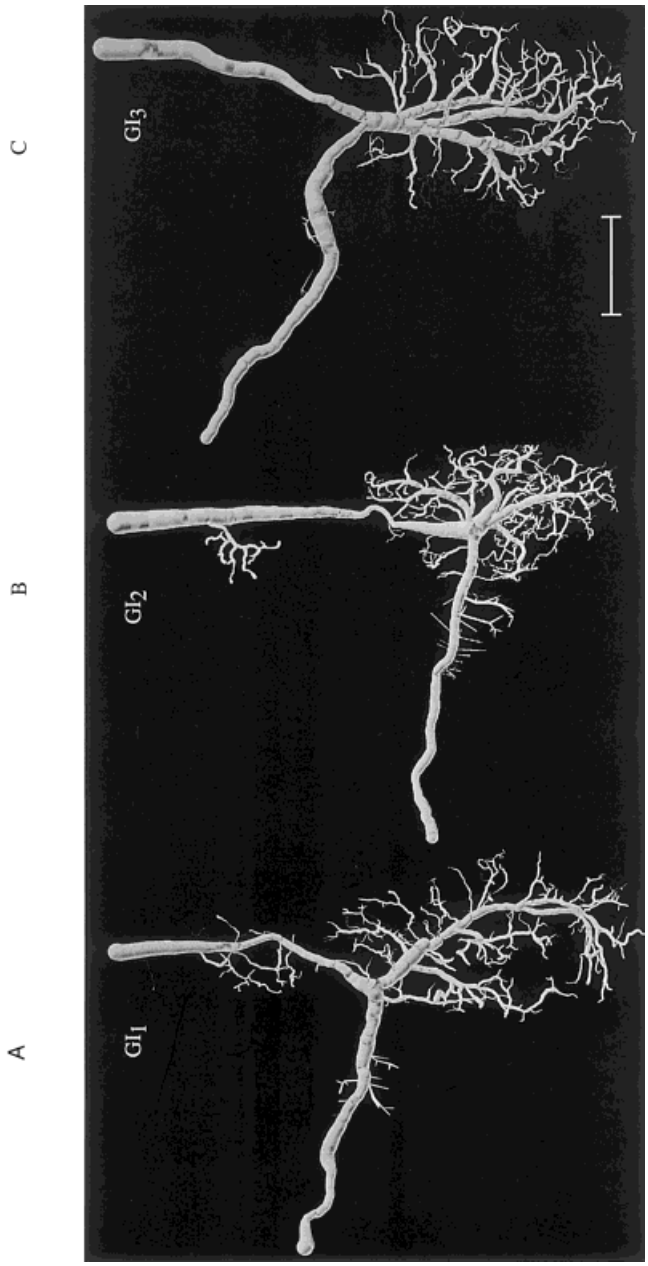

Figure 3

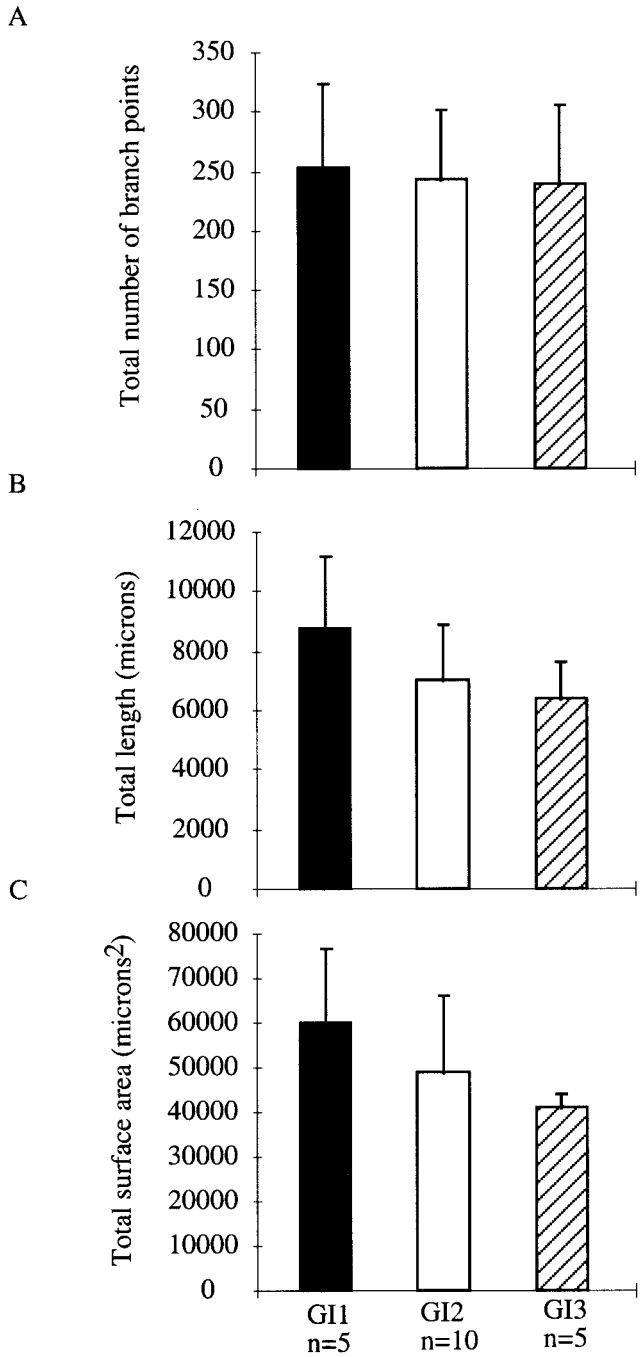

Fig. 4. Histograms of three metric parameters for the dendritic trees of the three GIs. **A:** Histogram showing the total number of branch points. **B:** Histogram showing the total length. **C:** Histograms showing the total surface area. None of these metric parameters was significantly different among the GIs (analysis of variance; $P > 0.05$).

for the intergroup is only 40% (Fig. 8, dashed line). This demonstrates that the HM can discriminate the geometric differences between these different cell types.

Bilateral symmetry of the central nervous system is a feature that offers the opportunity to test the HM method further, because one can examine the morphologic differences between a specific GI and its homologous contralateral counterpart. One such example is shown in Figure 9A for a pair of GI_2s that were stained in the same animal. Our rationale was that, if the HM is an efficient tool to compute differences between two geometric structures, then it should compute a greater difference between homologous neurons from different individuals than between homologous neurons from the same individual. We double stained and analyzed pairs of GI_2s from the same animal (n = 6 GI_2s from 3 animals). Figure 9A (left) shows a photomicrograph of two homologue GI_2s that were stained within a single animal. Figure 9A (right) shows an additional homologue pair from a different animal

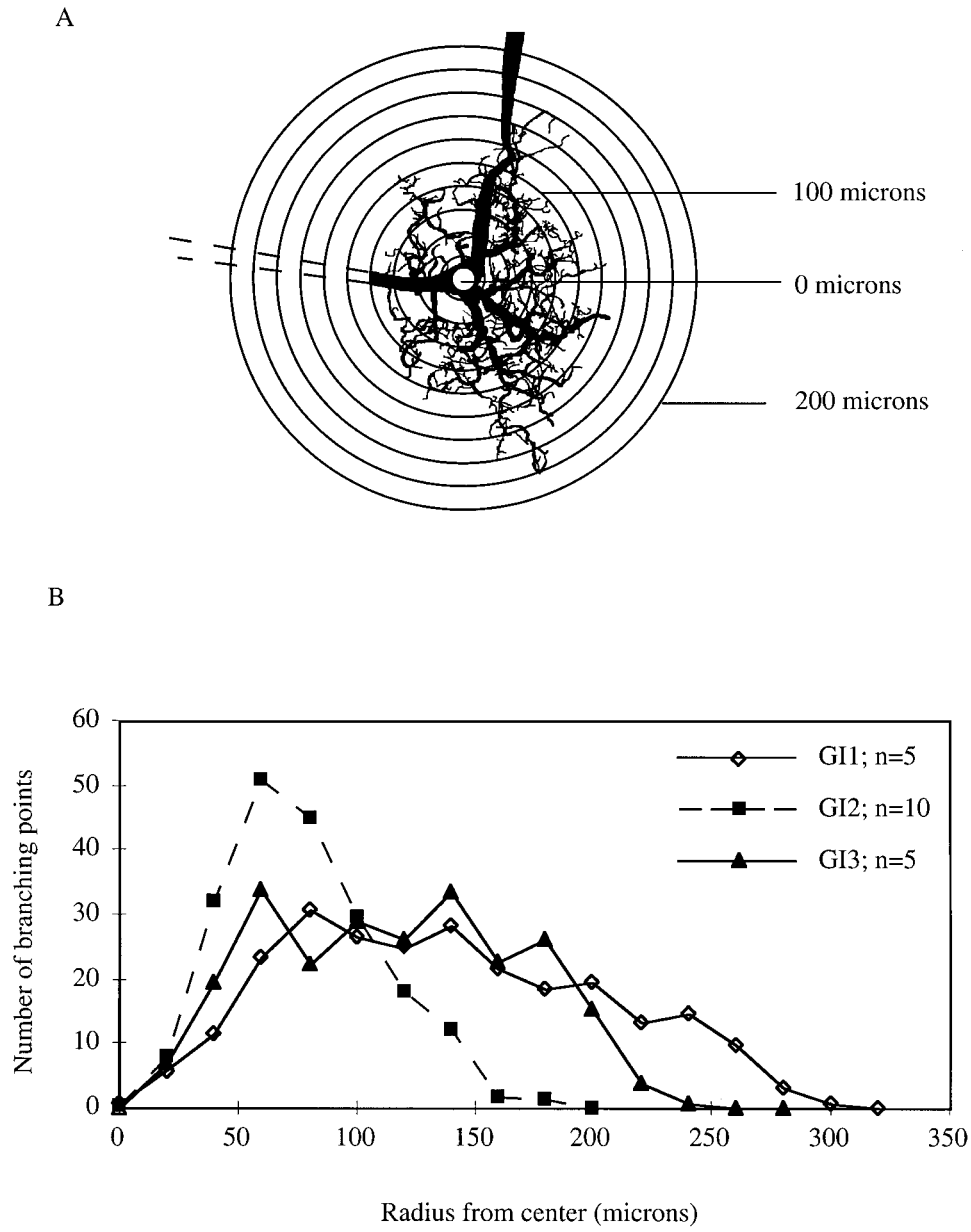

Fig. 5. Comparative analysis of the GIs using Sholl's concentric-spheres method. **A:** All neurons were aligned to the alignment node between the link segment, axon, and dendritic root. Concentric spheres spaced 20 μm apart were centered at this alignment node. **B:** Sholl plot for GI_1, GI_2, and GI_3 for the distribution of number of branch points along the dendritic field. Graph points represent average values.

after reconstruction. Analysis of the dendritic resemblance between cells from the same animal or from a different animal shows that homologue GI_2s (left vs. right) from the same animal show a higher degree of similarity (Fig. 9B, circles; data were calculated from 6 comparisons) than GI_2s from different animals (Fig. 9B, squares; data were calculated from 90 comparisons; $P < 0.01$; ANCOVA).

Standard morphometric analysis of the left-right homologous neurons is presented in Table 1. The variances in Table 1 are smaller than the variances of the histograms shown in Figure 4 (t-test; $P < 0.001$). Note that the morphometric parameters of the GI_2s that were stained as pairs had lower absolute values than those for single neurons. Parts of the dendritic trees of the two stained GI_2s overlapped in a small region of the neuropil. In this small region, the dendritic branches were not reconstructed. Thus, both the standard metrics and the HM tests showed higher similarities for homologous neurons from the same individual than from different individuals. In this case, the HM test reinforced the standard morphometric analysis.

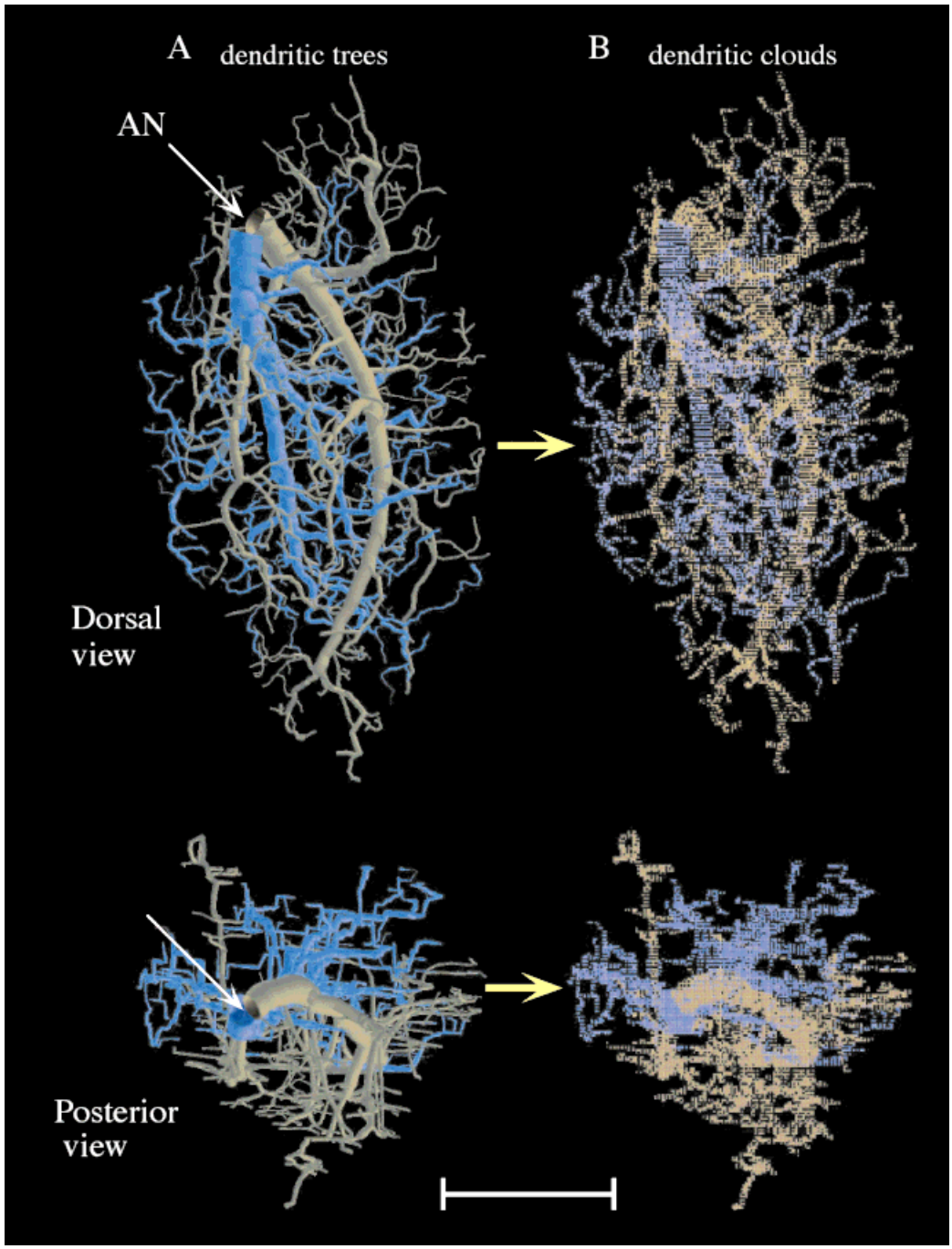

Fig. 6. Dendritic tree alignment and conversion into dendritic clouds for the Hausdorff match (HM) comparison. **A:** Dendritic trees of two GIs (GI_1, brown; GI_3, purple) aligned to their "alignment node" (AN; indicated by the white arrow). **B:** The dendritic trees shown in A after conversion into dendritic clouds (top, dorsal view; bottom, posterior view). Scale bar = 150 μm.

DISCUSSION

In this work, we have established a quantitative morphologic data base of three identified GIs. We chose these three neurons because their dendritic architecture is fairly similar. We quantitatively analyzed the similarity in their dendritic architecture by using a novel method based on the HD measure to compare pairs of dendritic trees.

Why a new metric?

One of the major problems in morphologic analysis of dendritic trees is the lack of a reliable measure for com-

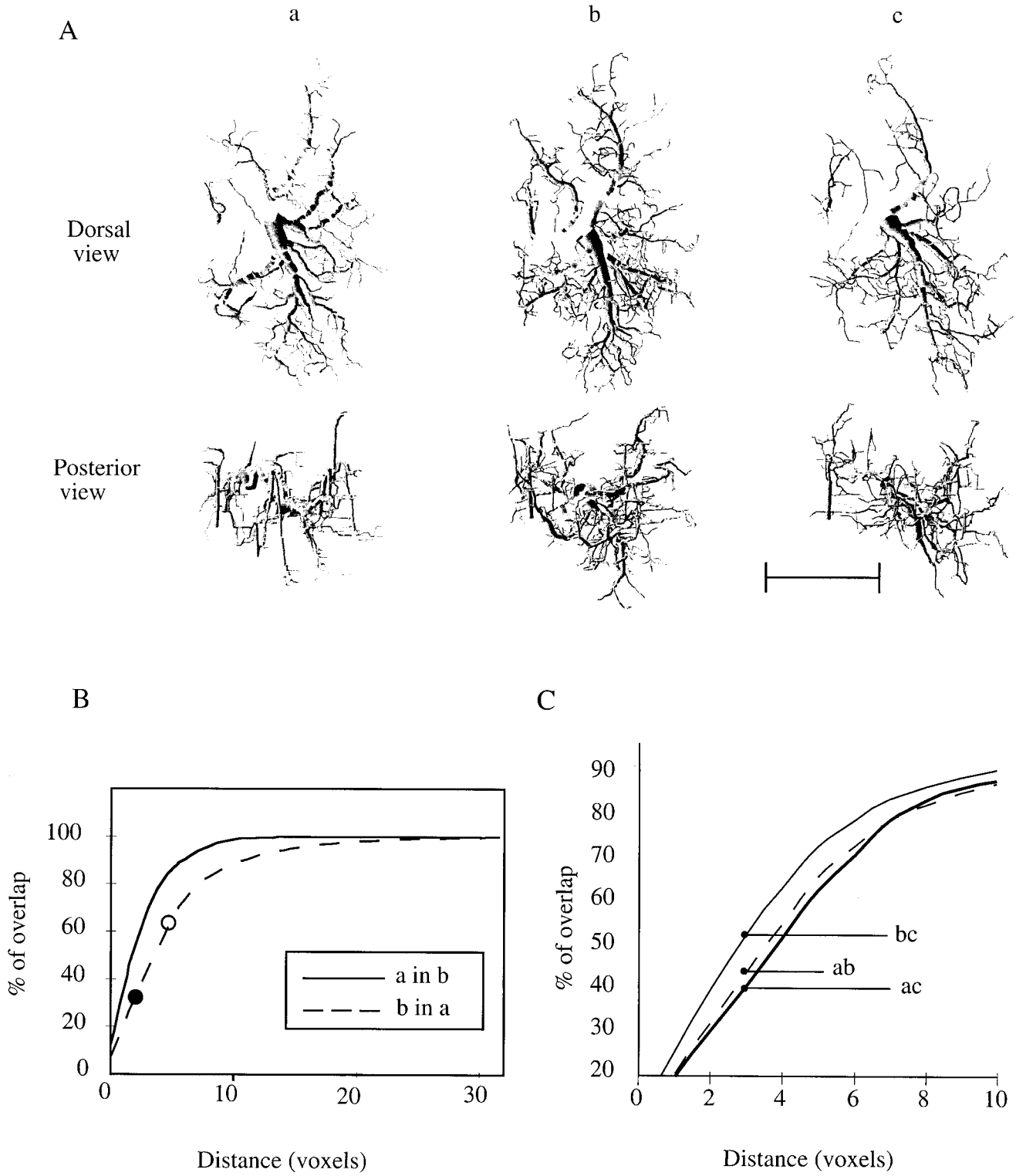

Fig. 7. HM comparison between dendritic trees. **A:** Three dendritic trees of GI_2 in the dorsal and posterior views (a–c; note that the axons are not drawn). **B:** Result curves of an HM comparison between dendritic tree a and dendritic tree b (from A). The solid line represents the comparison of "a in b," which yields better inclusion values than the "b in a" comparison (dashed line). Based on these two comparisons, we choose the curve with the lower values (i.e., "b in a") to be the symmetric HM result between dendritic trees a and b. At a voxel distance of 2, these two dendritic trees have 32% overlap (solid circle), whereas, at a voxel distance of 5, it increases to 62% (open circle). **C:** HM comparison of the three dendritic trees (a–c) from A. Dendritic trees b and c have higher resemblance ("bc" curve) than a and b ("ab" curve), or a and c ("ac" curve). Scale bar = 150 μm.

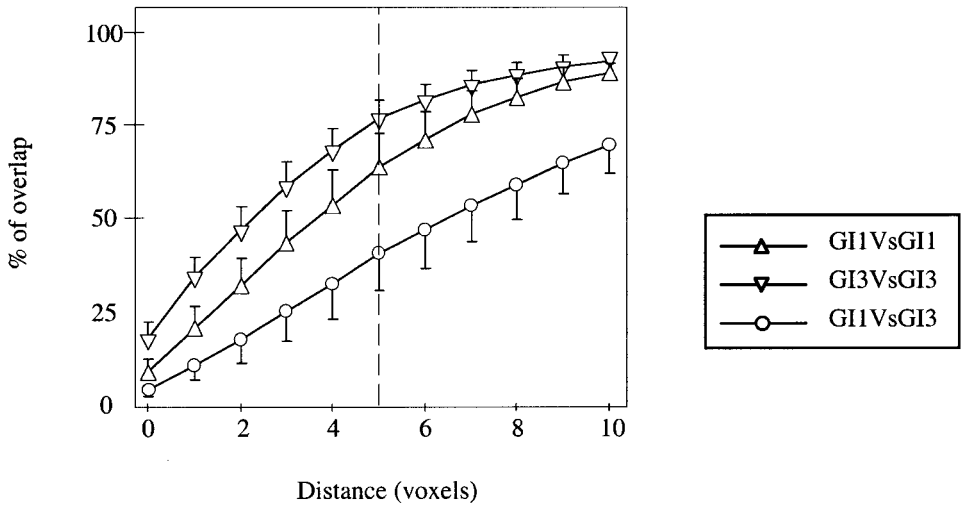

Fig. 8. HM comparison can discriminate between dendritic trees with different architecture. The graph plots the HM comparison curves for two groups of identified neurons (GI_1 and GI_3), within each group (GI_1 vs. GI_1 and GI_3 vs. GI_3; triangles), and between groups (GI_1 vs. GI_3; circles). The dashed line marks an ε-closeness at 5 voxels. At this distance, the intragroup similarity values are 63% and 76%, and the intergroup similarity is only 40%. The resemblance of the two intragroup curves are higher than the resemblance of the intergroup curve [analysis of covariance (ANCOVA); $P < 0.01$].

paring the geometry of these complex trees. The problem of comparing complex structures, such as dendritic and axonal trees, usually has been addressed by standard measures (length, surface area, number of branches, etc.). Although Sholl's analysis (Sholl, 1953) has been criticized because it combines topologic parameters with metric parameters and is not orientation-sensitive (Uylings et al., 1986), it is by far the most commonly used method for the spatial analysis of dendritic trees. The spatial orientation and density of dendritic trees also has been studied by using different methods, including "principal axes," "circular orientation," and "cartesian grid density" methods (Uylings et al., 1986). Such methods usually result only in general orientations of the dendritic tree where important geometric information is lost. More recently, methods based on fractal analysis have been developed and implemented to describe the complexity of dendritic trees (Smith et al., 1989, 1996; Caserta et al., 1995). A major disadvantage of all of these metric tools is that they do not discriminate between dendritic trees with similar degrees of complexity but different spatial morphologies. Jacobs and Theunissen (1996) recently presented a method to quantify the spatial distribution of the surface area of axonal varicosities. In this method, they used expected density functions to calculate several measures of the sensory neurons, such as the location and spatial extent of the arborization of a single afferent or the spatial segregation or overlap between the arborizations from several afferents. In our method, we also examine the anatomic overlap of arborizations. We aimed for a measure that was sensitive enough to discriminate between arborizations but also was insensitive to outliers. Here, an outlier is discarded automatically, because the HM finds the match that maximizes the percent of matching cloud points for each ε no matter how far the outlier is positioned relative to the voxel tested.

A dendritic tree occupies a very small volume relative to the volume of its bounding box (≈0.5%). Therefore, the probability that two dendritic trees will share a large percentage of the voxels is relatively low, even if the trees are very similar. On the other hand, because we align the root of the dendritic tree for comparing two neurons, the root region is expected to include cloud points of both neurons. Given these facts, we expect that, for small values of ε, we will receive small but significant P(A,B). Indeed, at $\varepsilon = 0$, the differences obtained are smaller than at larger ε values (Figs. 8, 9).

Live optical imaging and fluorescent methods have advanced tremendously in recent years. These methods allow the analysis of the same dendritic tree under different experimental treatments (Ziv and Smith, 1996; Wu and Cline, 1998; Engert and Bonhoeffer, 1999; Maletic-Savatic et al., 1999). Despite the appeal of live imaging, many problems remain to be solved. First, during acquisition, the cells experience photodamage and photobleaching. Second, the inability to perform histologic manipulations dramatically reduces the resolution of imaging live tissue versus fixed tissue. Third, the time window for the experiment is limited by the longevity of the preparation (which usually lasts from hours to a few days). Despite these limitations, using this "before-after" approach lowers the "noise" in the morphometric analysis that occurs when sampling neurons from different preparations. Nevertheless, automated comparative methods, like the HM approach, are appropriate tools to efficiently quantify and extract similarities and differences between such "before-after" dendritic pairs.

Identification of neuronal types versus identification of single neurons

Much like our ability to distinguish an oak tree from a cypress tree, the identification of neuronal types, such as a Purkinje neuron or a pyramidal neuron, is based on general appearance of the cell. Neuronal subtypes (pyramidal neurons from different fields of the hippocampus) are more difficult to identify and usually require quanti-

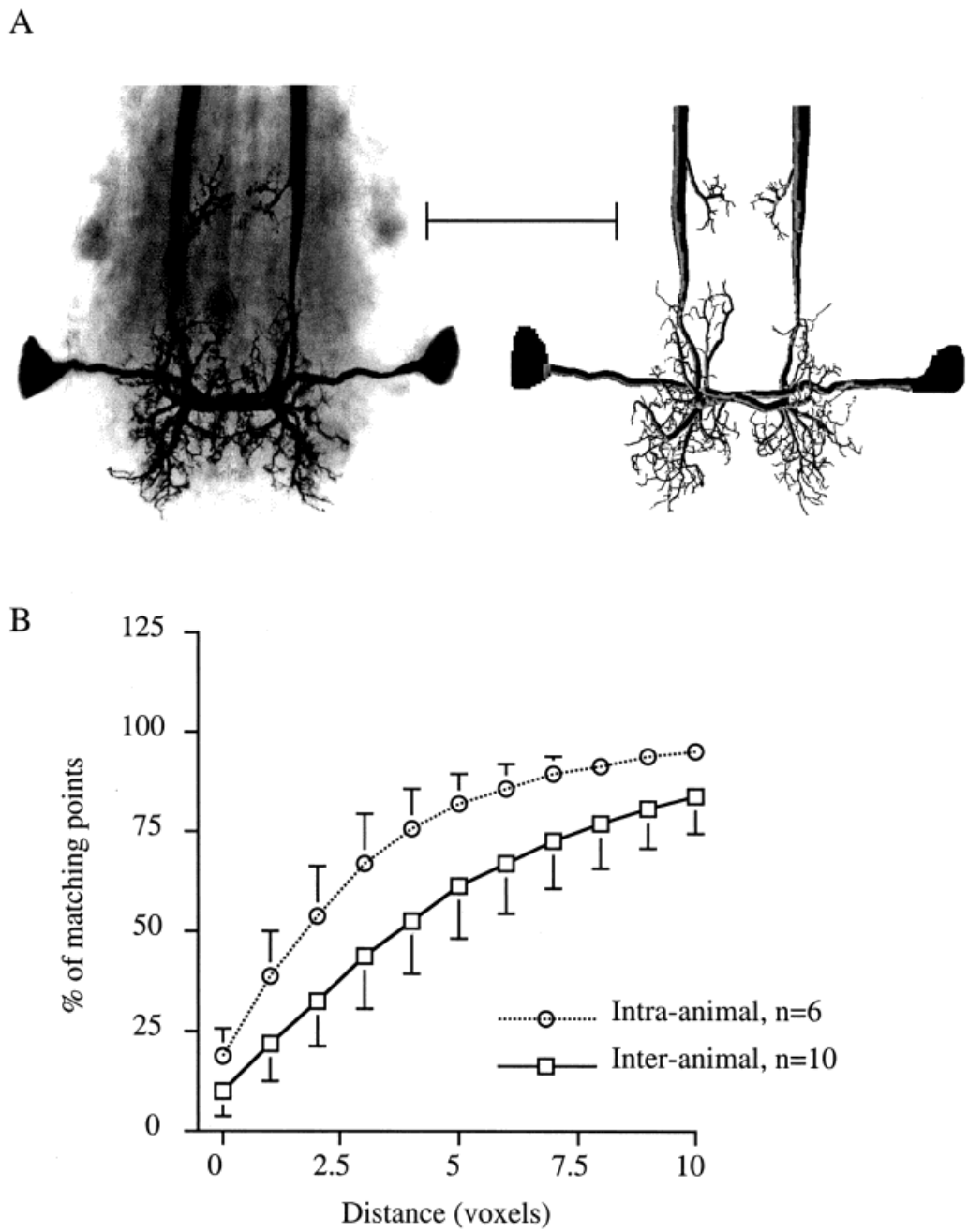

Fig. 9. **A:** Photomicrograph (left) of two homologous GI_2s from the same animal stained with neurobiotin. On the right is a reconstruction of a different pair of left and right GI_2s. **B:** HM comparisons of homologous GI_2 neurons from the same animal (intraanimal: n = 6 cells from 3 animals) and from different animals (interanimal: n = 10 cells from 10 animals). The intraanimal comparison curve is significantly higher than the interanimal comparison curve ($P < 0.01$). Scale bar = 200 μm.

tative support. Changes in dendritic structure of the same neuron are even more difficult to depict (Fig. 7). For example, Kolb et al. (1994) used statistical treatment and cluster analysis to identify three types of horizontal cells in the human retina from Golgi-impregnated neurons. Matesz et al. (1995) used multivariate statistical techniques to assess the morphologic identity of functionally different motoneurons in the frog. In this report, we introduce the HM measure as a method for classifying cells based on their 3D spatial morphology.

Although identified invertebrate neurons are defined as "constant" in their morphology and physiology across members of a given species, there is some morphologic variability in their architecture. Vertebrate neurons usually are not identified as individuals but as neuron subtypes from a given population. Such neurons also show

TABLE 1. Morphometric Parameters of Left and Right Pairs of Giant Interneuron 2

	Animal 1			Animal 2			Animal 3		
Measure	lGI2[1]	rGI2	Covariant	lGI2	rGI2	Covariant	lGI2	rGI2	Covariant
No. of branches	138	130	0.04	127	152	0.12	167	188	0.08
Total length (μm)	4,459	4,738	0.04	3,557	4,090	0.09	4,544	4,996	0.07
Surface area (μm^2)	34,460	32,340	0.05	29,288	32,263	0.07	35,128	40,252	0.10

[1]lGI2, left giant interneuron 2; rGI2, right giant interneuron 2.

striking similarities in general appearance. An interesting question is whether identifiable invertebrate neurons show a comparable degree of similarity to vertebrate neurons from a given subtype. For instance, the coefficients of variance of the total dendritic length for CA1, CA2, and CA3 pyramidal neurons of the rat were reported at 0.08, 0.06, and 0.24, respectively (Ishizuka et al., 1995), and at 0.20 for thalamocortical projection neurons of the cat (Ohara et al., 1995). These cells have total dendritic lengths that are comparable to those of the GIs (roughly 10,000 μm) but that do not seem less variable than the variability values we obtained (0.27, 0.26, and 019 for GI_1, GI_2, and GI_3, respectively). Quantitative comparison based on standard morphometric parameters is insufficient, as we have shown here. Future comparative work using the HM method will shed more light on this issue.

Variability of identified neurons

Although the dendritic branching patterns of neurons are very diverse, classes of neurons, such as pyramidal cells, share similar dendritic geometry. In the vertebrate brain, dissociated neurons of a given class, such as hippocampal pyramidal neurons, tend to redifferentiate dendritic arbors in vitro according to their morphology in vivo (Banker and Cowan, 1979). It is a well-established fact that invertebrate identified neurons show some morphologic variability. More specifically, the dendritic branching pattern of homologous, identified neurons shows some variability, indicating that dendritic architecture is not under strict genetic control (Macagno et al., 1973; Goodman, 1978; O'Shea et al., 1974; Hikosaka et al., 1996). These experiments reported that, although the locations of the major arborizations of an identified neuron occur with little variability, the fine pattern of dendritic branching is variable. Homologous, identified neurons within an animal are known to be more self similar than homologues from different animals, as shown in the optic system of daphnia (Macagno et al., 1973) and the visual neurons of grasshoppers (Goodman, 1978). Our HM analysis supports these previous qualitative observations by implementing quantitative measurements of similarity. Analysis of the dendritic resemblance between cells from the same animal with the HM method shows that homologous left and right GI_2s from the same animal exhibit a higher degree of similarity in their dendritic geometry than GI_2s from different animals. Thus, our results provide further support for the idea that dendritic architecture is the product of both intrinsic influences and extrinsic influences.

Limitations of the Hausdorff method

One may claim that the requirement to convert the dendritic segments into clouds of points in space is a disadvantage of the HM method (Fig. 6). During this conversion, topologic information regarding branching patterns is lost. Indeed, topologic variability is a complicated geometric problem that usually is addressed by morphometric parameters, such as tree order, tests for asymmetry, and vertex analysis (Verwer and van Pelt, 1986; van Pelt et al., 1992). Recently, van Pelt et al. (1997) developed a mathematical model to investigate topologic variability during neurite outgrowth. The topology of dendritic trees is an important issue in a complete morphologic analysis but is beyond the scope of the current study.

In conclusion, this study has shown that the HM method is a straightforward test to measure geometric similarity between dendritic trees.

ACKNOWLEDGMENTS

The authors thank Y. Manor and G. Haspel for critically reading early versions of this article. This work was supported by an equipment grant to F.L from the Israel Science Foundation (grant 9001/95). M.J.K. and K.K. were supported by the Israel Science Foundation founded by the Israel Academy of Sciences and Humanities. K.K. was supported by the Mary Upson Award, College of Engineering, Cornell University.

LITERATURE CITED

Bacon JP, Blagburn JM. 1992. Ectopic sensory neurons in mutant cockroaches compete with normal cells for central targets. Development 115:773–784.

Banker GA, Cowan WM. 1979. Further observations on hippocampal neurons in dispersed cell culture. J Comp Neurol 187:469–494.

Blagburn JM, Beadle DJ. 1982. Morphology of identified cercal afferents and giant interneurons in the hatching cockroach *Periplaneta americana*. J Exp Biol 97:421–426.

Blagburn JM, Sosa MA, Blanco RE. 1996. Specificity of identified central synapses in the embryonic cockroach: appropriate connections form before the onset of spontaneous afferent activity. J Comp Neurol 373: 511–528.

Caserta F, Eldred WD, Fernandez E, Hausman RE, Stanford LR, Bulderev SV, Schwarzer S, Stanley HE. 1995. Determination of fractal dimension of physiologically characterized neurons in two and three dimensions. J Neurosci Methods 56:133–144.

Chew LP, Kedem K. 1998. Getting around a lower bound for the minimum Hausdorff distance. Computat Geometry Theor Application 10:1–6.

Chew MT, Goodrich MT, Huttenlocher DP, Kedem K, Kleinberg JM, Kravetz D. 1997. Geometric pattern matching under Euclidean motion. Computat Geometry Theor Application 7:113–124.

Daley DL, Vardi N, Appignani B, Camhi JM. 1981. Morphology of the giant interneurons and cercal nerve projections of the American cockroach. J Comp Neurol 196:41–52.

Engert F, Bonhoeffer T. 1999. Dendritic spine changes associated with hippocampal long-term synaptic plasticity. Nature 399:66–70.

Goodman CS. 1978. Isogenic grasshoppers: genetic variability in the morphology of identified neurons. J Comp Neurol 182:681–706.

Hikosaka R, Takahashi M, Takahata M. 1996. Variability and invariability in the structure of an identified nonspiking interneuron of crayfish as revealed by three-dimensional morphometry. Zool Sci 13:69–78.

Hill ES, Blagburn JM. 1998. Indirect synaptic inputs from filiform hair

sensory neurons contribute to the receptive fields of giant interneurons in the first instar cockroach. J Comp Physiol A 183:467–476.

Huttenlocher DP, Kedem K. 1990. Computing the minimum Hausdorff distance for point sets under translation. Proceedings of the sixth ACM Symposium on Computational Geometry (The Association for Computing Machinery [ACM], Inc., NY, NY). p 340–349.

Huttenlocher DP, Kedem K, Sharir M. 1991. The upper envelope of voronoi surfaces and its applications. Discrete Computat Geometry 9:267–291.

Huttenlocher DP, Klanderman GA, Rucklidge WJ. 1993. Comparing images using the Hausdorff distance. IEEE Trans Pattern Anal Machine Intelligence 15:850–863.

Ishizuka N, Cowan WM, Amaral DG. 1995. A quantitative analysis of the dendritic organization of pyramidal cells in the rat hippocampus. J Comp Neurol 362:17–45.

Jacobs GA, Nevin R. 1991. Anatomical relationships between sensory afferent arborizations in the cricket cercal system. Anat Rec 231:563–572.

Jacobs GA, Theunissen FE. 1996. Functional organization of a neural map in the cricket cercal sensory system. J Neurosci 16:769–784.

Kolb H, Fernandez E, Schouten J, Ahnelt P, Linberg KA, Fisher SK. 1994. Are there three types of horizontal cells in the human retina? J Comp Neurol 343:370–386.

Libersat F. 1992. Modulation of flight by the giant interneurons of the cockroach. J Comp Physiol A 170:379–392.

Macagno ER, Lopresti V, Levinthal C. 1973. Structure and development of neuronal connections in isogenic organisms: variations and similarities in the optic system of *Daphnia magna*. Proc Natl Acad Sci USA 70:57–61.

Maletic-Savatic M, Malinow R, Svoboda K. 1999. Rapid dendritic morphogenesis in CA1 hippocampal dendrites induced by synaptic activity. Science 283:1923–1927.

Matesz C, Birinyi A, Kothalawala DS, Székely G. 1995. Investigation of the dendritic geometry of brain stem motoneurons with different functions using multivariant statistical techniques in the frog. Neuroscience 65:1129–1144.

Mendenhall B, Murphey RK. 1974. The morphology of cricket giant interneurons. J Neurobiol 5:565–580.

Mizrahi A, Ben-Ner E, Glusman JG, Katz M, Kedem K, Libersat F. 1999. Comparative analysis of dendritic architecture of identified neurons using the Hausdorff distance metric. Neurosci Lett Suppl 54:30.

Ohara PT, Ralston HJ III, Havton LA. 1995. Architecture of individual dendrites from intracellularly labeled thalamocortical projection neurons in the ventral posterolateral and ventral posteromedial nuclei of the cat. J Comp Neurol 358:563–572.

O'Shea M, Rowell CHF, Williams JLD. 1974. The anatomy of a locust visual interneuron; the descending contralateral movement detector. J Exp Biol 60:1–12.

Ritzmann RE. 1984. The cockroach escape response. In: Eaton R, editor. Neural mechanisms of startle behavior. New York: Plenum Press. p 93–131.

Segev I. 1992. Single neurone models: oversimple, complex and reduced. TINS 15:414–421.

Segev I, Rall W. 1998. Excitable dendrites and spines: earlier theoretical insights elucidate recent direct observations. Trends Neurosci 21:453–460.

Sholl DA. 1953. Dendritic organization in the neurons of the visual cortex and motor cortices of the cat. J Anat (London) 87:387–406.

Smith TG Jr., Marks WB, Lange GD, Sheriff WH Jr., Neale EA. 1989. A fractal analysis of cell images. J Neurosci Methods 27:173–180.

Smith TG Jr., Lange GD, Marks WB. 1996. Fractal methods and results in cellular morphology- dimensions, lacunarity and multifractals. J Neurosci Methods 69:123–136.

Uylings HBM, Ruiz-Marcos A, van Pelt J. 1986. The metric analysis of three dimensional dendritic tree patterns: a methodological review. J Neurosci Methods 18:127–151.

van Pelt J, Uylings BM, Verwer RWH, Pentney RJ, Woldenberg MJ. 1992. Tree asymmetry–a sensitive and practical measure for binary topological trees. Bull Math Biol 54:759–784.

van Pelt J, Dityatev AE, Uylings HB. 1997. Natural variability in the number of dendritic segments: model-based inferences about branching during neurite outgrowth. J Comp Neurol 387:325–340.

Verwer RWH, van Pelt J. 1986. Descriptive and comparative analysis of geometric properties of neuronal tree structures. J Neurosci Methods 18:179–206.

Wu GY, Cline HT. 1998. Stabilization of dendritic arbor structure in vivo by CaMKII. Science 279:222–226.

Yuste R, Tank DW. 1996. Dendritic integration in mammalian neurons, a century after Cajal. Neuron 16:701–716.

Ziv NE, Smith SJ. 1996. Evidence for a role of dendritic filopodia in synaptogenesis and spine formation. Neuron 17:91–102.